Development and Verification of a Novel Measurement and Position System for Confined Cabin

Qiang Hao, Guochen Wang, Pan Jiang, Dongkang Yu, Dan Wang, Ming Yang, and Dingjie Xu

***Abstract*—The high-accuracy key points measurement is necessary for shipbuilding, and numerous measuring systems have been invented. However, there are still limitations and challenges in measurement frequency, calibration method and environmental disturbances. This paper presents a novel and automatic measurement and position system based on laser scan technology. The system components and mathematical model are introduced. Subsequently, a fast calibration method is established, also different calibration schemes and calibration algorithms are discussed. To avoid the environmental disturbances to this system, a robust positioning algorithm based on maximum likelihood estimation is presented. A series of simulation and verification experiments in normal and interferential environment are designed to evaluate the precision of the proposed system. The results shows that the system's position accuracy can reach 1.00mm with 50Hz output whether there are disturbances or not, which can meet the need of position in the confined cabin.**

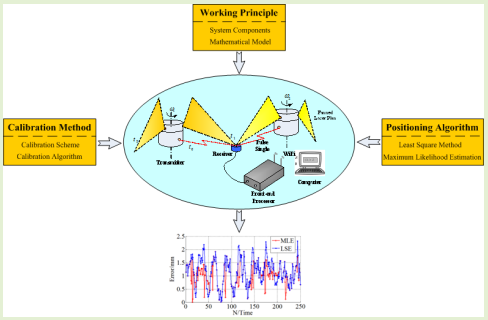

***Index Terms*—Shipbuilding, laser scan, fast calibration, robust algorithm, high precision position system.**

I. Introduction

THE measurement and position of key points inside ships has a huge influence on shipbuilding, such as cabin welding, piping installation, equipment layout and so on. To some extent, the measurement and position accuracy directly determines the construction quality, so tremendous efforts have been devoted to research on measurement and position methods. However, thanks to the space limitation of confined cabin, traditional methods usually use the manual measurement, for example, tapelines, total stations, laser tracker or other facilities, which cannot guarantee the accuracy and efficiency at the same time. Meanwhile, the conventional methods meet a huge challenge on account of the increasing demand for continuous measurement, because they can only provide a little discrete position information [1]–[4].

In order to improve the measurement quality and efficiency, obtain high-frequency measurement information in confined space, various methods have been developed and lots of systems have been invented. Among them, systems based on machine vision and systems based on laser scan show a bright future. In detail, the methods based on machine vision can be divided into three parts: photogrammetry, line-scan camera and structured light scanning. For example, Mendikute developed a self-calibrated in-process photogrammetry system [5]. The main innovations of this method lie in the optimized in-process joint bundle adjustment algorithm and the self-calibrated method for camera and lens distortion. With these novel methods the positioning accuracy can achieve 0.1 mm in 1m. However, to obtain a frequency output of 1Hz, there are lots of pictures to process at the same time which brings a fair amount of computation; also the quality of pictures determined the measurement accuracy directly, while the bad conditions in the cabin can't fully guarantee the quality. Sun presented a 3D coordinate measurement system based on dual line-scan cameras, and he introduced the basic working principle, the stereo configuration, the image matching strategy and calibration algorithm in detail, the experimental results showed a high accuracy at about 0.5mm [6], [7]. Unfortunately, the relative velocity of the line-scan camera and the point to be measured must be consistent, or else the resulting pictures will be stretched or compressed, which may introduce lots of errors or even cause measuring failure. At the same time, dual line-scan cameras time synchronization may also cause a series of problems; However, he doesn't conduct relevant methods study to deal with this problem. Hui has focused on the structured light scanning positioning

Manuscript received September 4, 2020; revised September 28, 2020; accepted September 28, 2020. Date of publication October 1, 2020; date of current version January 6, 2021. This work was supported in part by the Postdoctoral Foundation of Heilongjiang Province Government under Grant LBH-Z17091 and Grant LBH-Z17094, in part by the National Natural Science Foundation of China under Grant 51909048 and Grant 61573117, and in part by the China Postdoctoral Science Foundation under Grant 2019T120260. The associate editor coordinating the review of this article and approving it for publication was Prof. Kazuaki Sawada. *(Corresponding author: Guochen Wang.)*

The authors are with the Harbin Institute of Technology, Harbin 150001, China, and also with the China Ship Research and Development Academy, Beijing 100192, China (e-mail: wanggc@hit.edu.cn).

Digital Object Identifier 10.1109/JSEN.2020.3028093

study, and he invented a robot-integrated fringe projection scanning positioning system based on the structured light scanning system [8], [9]. The unified theory of multi-coordinate systems and a novel hand-eye calibration method based on synchronized observation algorithm have been researched in his paper, and the measuring accuracy of this system can reach 0.25mm. However, more efforts are needed in data fusion methods and path planning algorithm. To sum up, although machine vision can provide high measurement accuracy, it has problems such as large amount of calculation, strict environmental requirements and immature processing algorithm, which limits the application of this method. The laser scanning systems are based on the theodolite principle. By increasing the guiding mechanism, the high frequency and high precision measurement results can be obtained automatically. For instance, Zhang and Zhou presented an automatic guided laser theodolite system [10], [11]. The basic compositions of this system are two laser motorized theodolites to provide azimuth/pitch information of the measured points and a control guidance system to accomplish the target searching. Through studying the automatic guidance algorithm and establishing the discriminant tracking models, the measuring accuracy of this system can reach 0.3mm. However, the points to be measured may be unrecognizable if the features of these points can't match the discriminant tracking models, also the calibration between the theodolite coordinate system and the control guidance system coordinate system calibration costs a lot of time, which makes this system inefficient. In summary, both the machine vision method and laser scanning method have various shortcomings, so it is worthy to study a new system to achieve efficient, low environmental requirements, millimeter accuracy and high frequency output measurement and position.

In this paper, an accurate, flexible and automatic measurement system called ship high precision measuring and positioning system (SHPMPS) is proposed. This system is based on the laser scanning principle and it is composed by receivers, transmitters, front-end processors, calibration equipment and computers. The characteristics of this SHPMPS are as follows: Using two line lasers to determine the positions based on the theodolite principle; using a high-speed motor to drive the line lasers to scan the key points to achieve a high frequency output; using the calibration instrument to calibrate quickly; and finally achieving the automatic measurement of the key points whether there are external disturbances or not.

The remainder of this paper is organized as follows: Section 2 introduces how SHPMPS works in detail, also the accurate mathematical model is built in this part. Section 3 designs a fast calibration scheme and presents a novel calibration algorithm. Section 4 studies the robust positioning method under the circumstance of disturbances. A validity evaluation is presented in section 5, including simulation and verification experiments. At last, a conclusion is remarked in section 6.

II. Working Principle

A. System Components

The main components of the SHPMPS are shown in Fig.1. Since the calibration equipment doesn't participate in the positioning calculation, and its structure needs to be discussed in detail later, the calibration equipment is not shown in Fig.1. The receiver placed in the measured point is a photoelectric converter, and its main role is to receive optical signals from the transmitters and send electrical signals to the front-end processor. The transmitter is similar to a theodolite to some extent, whose task is to measure the receiver's azimuth and pitch angles relative to itself [12]. To be specific, two fanned laser planes with fixed angles (θ_{off}) which are emitted from the line lasers sweep through the whole space to be measured continuously, at the same time the stationary pulse lasers deliver pulse singles to the receiver as the transmitter's starting time (T_0) as soon as the laser plane1 turns a circle, also the singles are recorded when the two laser planes sweep over the receiver in turn. The front-end processor separates the signals from the line lasers and the pulse lasers, and calculates the time (T_1, T_2) when the receiver receives the signal from the two line laser. Then the scanning angles (θ_1, θ_2) of the two laser planes can be calculated based on the known rotating speed of the line lasers (ω), shown as Equations (1). The azimuth and pitch angles can be got according to the scanning angles, and the receiver's coordinates can be determined if the receiver receives signals from at least two transmitters. The receiver's coordinates are transmitted to the computer through WiFi and displayed in the computer.

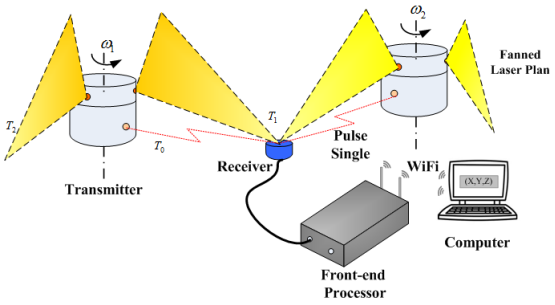

Fig. 1. System configuration.

According to Equations (1), if the rotating speed is quick enough, the rotating frequency will also be large, which will increase the amount of the scanning angles (θ_1, θ_2) in unit time. As a result, the system solution frequency has been enhanced, which ensures the highly efficient output of the system positioning results.

$$\begin{cases} \theta_1 = \omega (T_1 - T_0) \\ \theta_2 = \omega (T_2 - T_0) \end{cases} \tag{1}$$

B. Mathematical Model

The mathematical model is based on two important coordinate systems which are defined as follows (Fig. 2 and Fig. 3).

Transmitter coordinate system (marked as t): Z-axis is the transmitter's rotation axis which two laser planes rotate around. Origin is the intersection of laser plane 1 and Z-axis. X-axis is the intersecting line between the laser plane1 and the vertical plane of Z-axis when the laser plane 1 rotates to the starting time (T_0). Y-axis is determined according to the right-hand rule.

Global coordinate system (marked as g): The coordinate system is based on two transmitters. Z-axis and Origin are the Z-axis and Origin of transmitter 1's coordinate

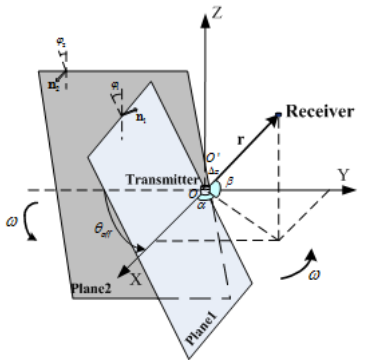

Fig. 2. Transmitter coordinate system.

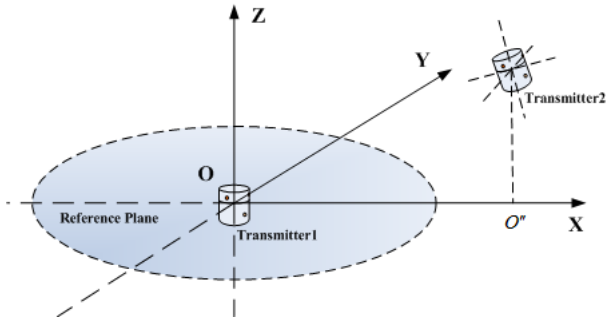

Fig. 3. Global coordinate system.

system respectively. Supposing that the projection point of transmitter 2 on the vertical plane of Z-axis is O'', and then X-axis is the connection between the Origin and O''. Also Y-axis is determined according to the right-hand rule.

The transformation relation between the two coordinate systems can be described as:

$$\begin{bmatrix} X_g \\ Y_g \\ Z_g \end{bmatrix} = \boldsymbol{R} \begin{bmatrix} X_t \\ Y_t \\ Z_t \end{bmatrix} + \boldsymbol{V} \tag{2}$$

where $\boldsymbol{R}$ is the rotation matrix which can be represented by three Euler angles, $\boldsymbol{V}$ is the translation matrix which consists of the transmitter's coordinates in global coordinate system. We define $\boldsymbol{R}$ and $\boldsymbol{V}$ as external parameters in this paper and these external parameters can be determined by calibrating which we will describe in detail later.

Besides, there are some basic parameters in the transmitter coordinate system. According to Fig. 2, φ_1, φ_2 are the inclined angles between laser plane 1, 2 and Z-axis, and θ_{off} is a fixed offset angle between the two laser planes. Since two laser plans and the Z-axis cannot intersect at one point (the Origin) in the transmitter coordinate system because of the assembly error, and we suppose the laser plan 2 intersects the Z-axis at O', then Δz is defined as the distance between the Origin and the O'. These parameters (φ_1, φ_2, θ_{off}, Δz) can be regarded as internal parameters, since they only depend on the assembly process, they can be treated as constants as soon as the transmitter is completed.

Based on the coordinate systems and external/ internal parameters defined above, there are two ways to calculate the coordinates of the key points: Azimuth/pitch angles measuring according to the theodolite principle and bundle adjustment based on the photogrammetry. Two methods are described as below.

1) Azimuth/Pitch Angles Measuring: When the laser plane 1 rotates to the starting time T_0, the normal vectors of the two planes can be expressed as Equations (3) and Equations (4) in transmitter coordinate system:

$$\vec{\boldsymbol{n}}_1^{\boldsymbol{0}} = \begin{bmatrix} 1 & 0 & 0 \\ 0 & \cos\varphi_1 & -\sin\varphi_1 \\ 0 & \sin\varphi_1 & \cos\varphi_1 \end{bmatrix} \begin{bmatrix} 0 \\ 1 \\ 0 \end{bmatrix} = \begin{bmatrix} 0 \\ \cos\varphi_1 \\ \sin\varphi_1 \end{bmatrix} \tag{3}$$

$$\begin{aligned} \vec{\boldsymbol{n}}_2^{\boldsymbol{0}} &= \begin{bmatrix} \cos\theta_{off} & -\sin\theta_{off} & 0 \\ \theta_{off} & \cos\theta_{off} & 0 \\ 0 & 0 & 1 \end{bmatrix} \begin{bmatrix} 0 \\ \cos\varphi_2 \\ \sin\varphi_2 \end{bmatrix} \\ &= \begin{bmatrix} -\sin\theta_{off}\cos\varphi_2 \\ \cos\theta_{off}\cos\varphi_2 \\ \sin\varphi_2 \end{bmatrix} \end{aligned} \tag{4}$$

When the two laser planes sweep over the receiver at time T_1 and T_2 in turn, the normal vectors change into:

$$\vec{\boldsymbol{n}}_1^{\boldsymbol{T}} = \begin{bmatrix} \cos\theta_1 & -\sin\theta_1 & 0 \\ \sin\theta_1 & \cos\theta_1 & 0 \\ 0 & 0 & 1 \end{bmatrix} \vec{\boldsymbol{n}}_1^{\boldsymbol{0}} = \begin{bmatrix} -\sin\theta_1\cos\varphi_1 \\ \cos\theta_1\cos\varphi_1 \\ \sin\varphi_1 \end{bmatrix} \tag{5}$$

$$\begin{aligned} \vec{\boldsymbol{n}}_2^{\boldsymbol{T}} &= \begin{bmatrix} \cos\theta_2 & -\sin\theta_2 & 0 \\ \sin\theta_2 & \cos\theta_2 & 0 \\ 0 & 0 & 1 \end{bmatrix} \vec{\boldsymbol{n}}_2^{\boldsymbol{0}} \\ &= \begin{bmatrix} -\sin\left(\theta_2+\theta_{off}\right)\cos\varphi_2 \\ \cos\left(\theta_2+\theta_{off}\right)\cos\varphi_2 \\ \sin\varphi_2 \end{bmatrix} \end{aligned} \tag{6}$$

where θ_1 and θ_2 can be obtained by Equations (1).

The unit direction vector $\vec{\boldsymbol{r}}_{\boldsymbol{t}}$ from the Origin to the receiver can be expressed as Equations (7) using the azimuth angle α and pitch angle β (Shown as Fig.2).

$$\vec{\boldsymbol{r}}_{\boldsymbol{t}} = \begin{bmatrix} \cos\alpha\cos\beta & \sin\alpha\cos\beta & \sin\beta \end{bmatrix} \tag{7}$$

where $\vec{\boldsymbol{r}}_{\boldsymbol{t}}$ is defined in the transmitter coordinate system.

When the two laser planes sweep over the receiver respectively, there are $\vec{\boldsymbol{r}}_{\boldsymbol{t}} \perp \vec{\boldsymbol{n}}_{\boldsymbol{1}}^{\boldsymbol{t}}$, $\vec{\boldsymbol{r}}_{\boldsymbol{t}} \perp \vec{\boldsymbol{n}}_{\boldsymbol{2}}^{\boldsymbol{t}}$, namely:

$$\begin{cases} \vec{\boldsymbol{r}}_{\boldsymbol{t}} \cdot \vec{\boldsymbol{n}}_{\boldsymbol{1}}^{\boldsymbol{T}} = 0 \\ \vec{\boldsymbol{r}}_{\boldsymbol{t}} \cdot \vec{\boldsymbol{n}}_{\boldsymbol{2}}^{\boldsymbol{T}} = 0 \end{cases} \tag{8}$$

According to Equations (8), the azimuth angle α and pitch angle β can be calculated:

$$\begin{cases} \alpha = \arctan\left(\dfrac{\sin\theta_1\tan\varphi_2 - \sin\left(\theta_2+\theta_{off}\right)\tan\varphi_1}{\cos\theta_1\tan\varphi_2 - \cos\left(\theta_2+\theta_{off}\right)\tan\varphi_1}\right) \\ \beta = \arctan\left(\dfrac{\sin\left(\theta_1-\alpha\right)}{\tan\varphi_1}\right) \end{cases} \tag{9}$$

Or:

$$\begin{cases} \alpha = \arctan\left(\dfrac{\sin\theta_1\tan\varphi_2 - \sin\left(\theta_2+\theta_{off}\right)\tan\varphi_1}{\cos\theta_1\tan\varphi_2 - \cos\left(\theta_2+\theta_{off}\right)\tan\varphi_1}\right) + \pi \\ \beta = \arctan\left(\dfrac{\sin\left(\theta_1-\alpha\right)}{\tan\varphi_1}\right) \end{cases} \tag{10}$$

The reason why there are two solutions is the intersection line of the planes in space is a straight line passing through the

Origin, so there is a virtual receiver that's symmetric with the true receiver. We can judge the true receiver by the following formula.

$$\left[\vec{\boldsymbol{r}}_{\boldsymbol{t}} \times \left(\vec{\boldsymbol{n}}_{\mathbf{1}}^{\boldsymbol{T}}\right)^{T}\right] \cdot (0,0,1)^{T} > 0 \tag{11}$$

According to the theodolite measuring principle, if a receiver receives signals from at least two transmitters, the receiver coordinates $\boldsymbol{X}_{\boldsymbol{g}}^{\boldsymbol{r}}\left[X_{gx}^{r}, X_{gy}^{r}, X_{gz}^{r}\right]^{T}$ can be calculated using the following formulas.

$$\vec{\boldsymbol{r}}_{\boldsymbol{g}}^{\boldsymbol{n}} = \boldsymbol{R}^{\boldsymbol{n}} \cdot \vec{\boldsymbol{r}}_{\boldsymbol{t}}^{\boldsymbol{n}} \tag{12}$$

$$\begin{cases} \frac{X_{1x}-X_{gx}^{r}}{r_{gx}^{1}} = \frac{X_{1y}-X_{gy}^{r}}{r_{gy}^{1}} = \frac{X_{1z}-X_{gz}^{r}}{r_{gz}^{1}} \\ \frac{X_{2x}-X_{gx}^{r}}{r_{gx}^{2}} = \frac{X_{2y}-X_{gy}^{r}}{r_{gy}^{2}} = \frac{X_{2z}-X_{gz}^{r}}{r_{gz}^{2}} \\ \vdots \\ \frac{X_{nx}-X_{gx}^{r}}{r_{gx}^{n}} = \frac{X_{ny}-X_{gy}^{r}}{r_{gy}^{n}} = \frac{X_{nz}-X_{gz}^{r}}{r_{gz}^{n}} \end{cases} \tag{13}$$

where $\boldsymbol{X}_{\boldsymbol{n}}\left[X_{nx}, X_{ny}, X_{nz}\right]^{T}$ is the transmitter coordinates, and $\vec{\boldsymbol{r}}_{\boldsymbol{g}}^{\boldsymbol{n}} = \left[r_{gx}^{n}, r_{gy}^{n}, r_{gz}^{n}\right]$ is the unit direction vector in the global coordinate system. $\boldsymbol{R}^{\boldsymbol{n}}$ is the rotation matrix. The symbol n in $\boldsymbol{X}_{\boldsymbol{n}}$, $\vec{\boldsymbol{r}}_{\boldsymbol{g}}^{\boldsymbol{n}}$ and $\boldsymbol{R}^{\boldsymbol{n}}$ is the number of transmitters.

Equations (13) can be arranged in the following form if $n \geq 2$:

$$\boldsymbol{A}\boldsymbol{X}_{\boldsymbol{g}}^{\boldsymbol{r}} = \boldsymbol{B} \tag{14}$$

Then the receiver coordinates $\boldsymbol{X}_{\boldsymbol{g}}^{\boldsymbol{r}}$ can be calculated based on the least square estimation (LSE) as shown in Equations (15).

$$\boldsymbol{X}_{\boldsymbol{g}}^{\boldsymbol{r}} = \left(\boldsymbol{A}^{\boldsymbol{T}}\boldsymbol{A}\right)^{-1}\boldsymbol{A}^{\boldsymbol{T}}\boldsymbol{B} \tag{15}$$

2) Bundle Adjustment: The bundle adjustment is realized by establishing the plane parameter equation shown as Equations (16) [13]–[15].

$$\begin{cases} a_1^t X_{gx}^r + b_1^t X_{gy}^r + c_1^t X_{gz}^r + d_1^t = 0 \\ a_2^t X_{gx}^r + b_2^t X_{gy}^r + c_2^t X_{gz}^r + d_2^t = 0 \end{cases} \tag{16}$$

$\left[a_1^t, b_1^t, c_1^t, d_1^t\right]^T$ and $\left[a_2^t, b_2^t, c_2^t, d_2^t\right]^T$ are the two laser planes' parameters when the laser plane sweep over the receiver, respectively. In the transmitter coordinate system, they can be defined as follows based on Equations (5) and Equations (6).

$$\begin{bmatrix} a_1^t \\ b_1^t \\ c_1^t \\ d_1^t \end{bmatrix} = \begin{bmatrix} -\sin\theta_1 \cos\varphi_1 \\ \cos\theta_1 \cos\varphi_1 \\ \sin\varphi_1 \\ 0 \end{bmatrix} \tag{17}$$

$$\begin{bmatrix} a_2^t \\ b_2^t \\ c_2^t \\ d_2^t \end{bmatrix} = \begin{bmatrix} -\sin\left(\theta_2 + \theta_{off}\right)\cos\varphi_2 \\ \cos\left(\theta_2 + \theta_{off}\right)\cos\varphi_2 \\ \sin\varphi_2 \\ -\Delta z \cdot \sin\varphi_2 \end{bmatrix} \tag{18}$$

According to Equations (2), $\left[a_1^t, b_1^t, c_1^t, d_1^t\right]^T$ and $\left[a_2^t, b_2^t, c_2^t, d_2^t\right]^T$ can be transformed into the global coordinate system.

$$\begin{bmatrix} a_1^g \\ b_1^g \\ c_1^g \\ d_1^g \end{bmatrix} = \left[\begin{bmatrix} \boldsymbol{R} & \boldsymbol{V} \\ \mathbf{0} & \mathbf{1} \end{bmatrix}^{-1}\right]^T \begin{bmatrix} a_1^t \\ b_1^t \\ c_1^t \\ d_1^t \end{bmatrix} \tag{19}$$

$$\begin{bmatrix} a_2^g \\ b_2^g \\ c_2^g \\ d_2^g \end{bmatrix} = \left[\begin{bmatrix} \boldsymbol{R} & \boldsymbol{V} \\ \mathbf{0} & \mathbf{1} \end{bmatrix}^{-1}\right]^T \begin{bmatrix} a_2^t \\ b_2^t \\ c_2^t \\ d_2^t \end{bmatrix} \tag{20}$$

where $\left[a_1^g, b_1^g, c_1^g, d_1^g\right]^T$ and $\left[a_2^g, b_2^g, c_2^g, d_2^g\right]^T$ are the two laser planes' parameters of transmitter in the global coordinate system.

If there are at least two transmitters sweep over the receiver, the receiver coordinates $\boldsymbol{X}_{\boldsymbol{g}}^{\boldsymbol{r}}\left[X_{gx}^{r}, X_{gy}^{r}, X_{gz}^{r}\right]^{T}$ can be calculated using the following formulas.

$$\begin{cases} a_{11}^g X_{gx}^r + b_{11}^g X_{gy}^r + c_{11}^g X_{gz}^r + d_{11}^g = 0 \\ a_{12}^g X_{gx}^r + b_{12}^g X_{gy}^r + c_{12}^g X_{gz}^r + d_{12}^g = 0 \\ \vdots \\ a_{n1}^g X_{gx}^r + b_{n1}^g X_{gy}^r + c_{n1}^g X_{gz}^r + d_{n1}^g = 0 \\ a_{n2}^g X_{gx}^r + b_{n2}^g X_{gy}^r + c_{n2}^g X_{gz}^r + d_{n2}^g = 0 \end{cases} \tag{21}$$

The symbol n is the number of transmitters.

Also Equations (21) can be rewritten as the format like Equations (14) and the receiver coordinates can be calculated based on Equations (15).

3) Comparison of the Two Methods: In theory, the nature of the two methods is the same, the difference lies in the form of expression. The azimuth/pitch angles measuring uses the collinear method to calculate the receiver coordinates and the bundle adjustment uses the coplanar method. The advantage of the azimuth/pitch angles measuring is easy to understand because it is based on the theodolite measuring principle, and the advantage of the bundle adjustment is easy to calculate and the assembly error can be got at the same time, which is more practical. So we choose the bundle adjustment to realize the calculating of the receiver coordinates in subsequent chapters.

III. Calibration Method

According to the working principle of the SHPMPS, the purpose of calibration is to determine the internal and external parameters, and the easiest way to realize calibration is to construct constraint equations. So the core problems are the calibration scheme and the calibration algorithm.

A. Fast Calibration Scheme

The internal parameters are usually determined by other high-precision equipment during assembling, so they can be regarded as known parameters. However, there are slightly changed caused by vibration, transportation or even equipment aging. Therefore, it is of great importance to re-calibrate the internal parameters before measuring. Also the rotation matrix $\boldsymbol{R}$ and the translation matrix $\boldsymbol{V}$ should be calibrated after the measuring system is built.

If there are m receivers and n transmitters in the space to be measured, according to Equations (17) - Equations (20), Equations (21) can be arranged into the following matrix form.

$$\boldsymbol{K_n}\begin{bmatrix} \boldsymbol{R_n} & \boldsymbol{V_n} \\ \boldsymbol{0_{1\times 3}} & \boldsymbol{1} \end{bmatrix}^{-1} \boldsymbol{X_m} = \boldsymbol{0_{2\times 1}} \tag{22}$$

$\boldsymbol{K_n}$ is Transmitter n's coefficient matrix, shown as Equations (23). $\boldsymbol{R_n}$ and $\boldsymbol{V_n}$ are Transmitter n's rotation matrix and translation matrix, respectively.$\boldsymbol{X_m} = \left[X^r_{mgx}, X^r_{mgy}, X^r_{mgz}, 1\right]^T$ is Receiver m's coordinates in the global coordinate system.

$$\begin{aligned} \boldsymbol{K_n^T} &= [k_{n1}, k_{n2}] = \begin{bmatrix} a^t_{n1}, b^t_{n1}, c^t_{n1}, d^t_{n1} \\ a^t_{n2}, b^t_{n2}, c^t_{n2}, d^t_{n2} \end{bmatrix}^T \\ &= \begin{bmatrix} -\sin\theta_{n1}\cos\varphi_{n1}, -\sin\left(\theta_{n2}+\theta_{n,off}\right)\cos\varphi_{n2} \\ \cos\theta_{n1}\cos\varphi_{n1}, \cos\left(\theta_{n2}+\theta_{n,off}\right)\cos\varphi_{n2} \\ \sin\varphi_{n1}, \sin\varphi_{n2} \\ 0, -\Delta z_n\cdot\sin\varphi_{n2} \end{bmatrix} \end{aligned} \tag{23}$$

According to Equations (22) and Equations (23), there are $10n+3m$ unknown parameters in total, in detail, there are $4n$ internal parameters, $6n$ external parameters, and $3m$ receivers' three-dimensional coordinates in global coordinate system, respectively. Meanwhile, there are $2mn$ constraint equations if all receivers can receive all transmitters' signals. Additionally, if we know the distance between two receivers, there are $m(m-1)/2$ constraint equations shown as Equations (24).

$$\left\|\boldsymbol{X_i} - \boldsymbol{X_j}\right\|_2 = d_{i,j} \tag{24}$$

$\boldsymbol{X_m}$ is the receiver's coordinates in global coordinate system, $i, j \in [1, m]$ and $i \neq j$. $d_{i,j}$ is the known distance between receiver i and receiver j. $\|X\|_2$ is the l_2-norm.

To realize calibration, the relative quantity relationship between the receivers and transmitters can be expressed as Equations (25) based on Equations (22) - Equations (24).

$$2mn + \frac{m(m-1)}{2} \geq 10n + 3m \tag{25}$$

We can get the following results from Equations (25) (Take two transmitters' calibration as an example).

(1) If the receivers' coordinates are known, and we don't use the distance constrains, Equations (25) can be rewritten as $2mn \geq 10n$. So as long as there are at least five receivers in the space to be measured, the calibration can be completed regardless of the number of transmitters;

(2) If the receivers' coordinates are known, and we use the distance constrains, Equations (25) can be rewritten as $2mn + m(m-1)/2 \geq 10n$. So we need at least four receivers to realize calibration of two transmitters;

(3) If the receivers' coordinates are unknown, and the distance constrains can be used, according to Equations (25), we need at least six receivers to realize calibration of two transmitters;

(4) If the receivers' coordinates are unknown, and the distance constrains can't be used, either, Equations (25) can be rewritten as $2mn \geq 10n + 3m$. So we need at least twenty receivers to realize calibration of two transmitters.

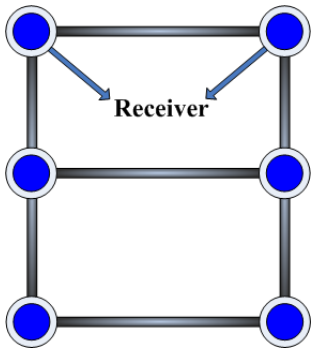

Fig. 4. Calibration equipment model.

Considering the narrow volume of the cabin, it is not suitable to use a large number of receivers to complete calibration. In addition, distance information is easier to obtain than receivers' coordinates information, so we choose the distance constrains to realize calibration.

Based on the analysis above, the calibration equipment can be designed as shown in Fig. 4. There are six receivers fixing on the frame, and the relative distance between each receiver is determined by the laser tracker. It should be noted that during the whole calibration process, all receivers in the calibration equipment must make sure of receiving the signals from every transmitter.

B. Calibration Algorithm

According to the calibration scheme, the main purpose of calibration algorithm is to solve Equations (22) and Equations (24). Combined with the calibration equipment model, calibration equations can be rewritten as follows:

$$\begin{cases} \boldsymbol{K_n}\begin{bmatrix} \boldsymbol{R_n} & \boldsymbol{V_n} \\ \boldsymbol{0_{1\times 3}} & \boldsymbol{1} \end{bmatrix}^{-1} \boldsymbol{X_m} = 0 \\ \left\|\boldsymbol{X_i} - \boldsymbol{X_j}\right\|_2 - d_{i,j} = 0 \end{cases} \tag{26}$$

where $n \in [1, 2]$, $m, i, j \in [1, 6]$ and $i \neq j$.

Equations (26) is a large-scale nonlinear equation with 39 equations and 38 unknown parameters, and how to accurately obtain these parameters needs further study. There are usually two ways to solve this equation: Function approximation algorithm and meta-heuristic algorithm. Function approximation algorithm includes Newton-Raphson method, Levenberg-Marquardt algorithm (L-M), Gauss-Newton method and so on [16]–[18]. Among them, L-M algorithm is the most widely used algorithm due to its characteristics of low local extremum probability, strong stability and fast convergence; Meta-heuristic algorithm includes simulated annealing, genetic algorithm, particle swarm optimization (PSO) and so on, and comparing with other algorithms, PSO has the advantages of easy implementation, high precision and fast convergence [19]–[21]. In this paper, we present two calibration algorithm based on L-M and PSO, and the final calibration algorithm is determined by comparing the advantages and disadvantages of the two methods.

1) Calibration Algorithm Based on L-M: L-M is an effective method for solving nonlinear equations. It is an improved Gauss-Newton method, which has both the local convergence of Newton method and the global search characteristic of

steepest descent method. Based on these benefits, the algorithm can converge effectively. The calibration algorithm based on L-M is outlined below.

The unknown parameters are written in matrix form as follows.

$$\begin{aligned} \boldsymbol{W} = \Big[&\varphi_{11}, \varphi_{12}, \theta_{1,off}, \Delta z_1, \varphi_{21}, \varphi_{22}, \theta_{2,off}, \Delta z_2, \\ &X_{1x}, X_{1y}, X_{1z}, X_{2x}, X_{2y}, X_{2z}, \Psi_1, \Phi_1, \\ &\Omega_1, \Psi_2, \Phi_2, \Omega_2, X^r_{1gx}, X^r_{1gy}, X^r_{1gz}, \cdots, X^r_{mgx}, \\ &X^r_{mgy}, X^r_{mgz}, \cdots, X^r_{6gx}, X^r_{6gy}, X^r_{6gz}\Big]^T \end{aligned} \tag{27}$$

where $[\Psi, \Phi, \Omega]$ are the inclination angle, pitch angle and roll angle of rotation matrix R.

Supposing $e_{m,n,1} = \boldsymbol{k_{n1}} \begin{bmatrix} \boldsymbol{R_n}, \boldsymbol{V_n} \\ \boldsymbol{0_{1\times 3}}, \boldsymbol{1} \end{bmatrix}^{-1} \boldsymbol{X_m}, e_{m,n,2} = \boldsymbol{k_{n2}} \begin{bmatrix} \boldsymbol{R_n}, \boldsymbol{V_n} \\ \boldsymbol{0_{1\times 3}}, \boldsymbol{1} \end{bmatrix}^{-1} \boldsymbol{X_m}$, $l_{i,j} = \|\boldsymbol{X_i} - \boldsymbol{X_j}\|_2 - d_{i,j}$, then the error matrix $\boldsymbol{e}(\boldsymbol{W})$ and the error performance function $\mathbf{E}(\boldsymbol{W})$ at time k are shown as follows.

$$\begin{aligned} \boldsymbol{e_k}(\boldsymbol{W}) = \Big[&e_{1,1,1,k}, e_{1,1,2,k}, \cdots, e_{m,n,1,k}, e_{m,n,2,k}, \cdots, \\ &e_{6,2,1,k}, e_{6,2,2,k}, l_{1,1,k}, \cdots, l_{i,j,k}, \cdots, l_{5,6,k}\Big]^T \end{aligned} \tag{28}$$

$$\mathbf{E_k}(\boldsymbol{W}) = \frac{1}{2}\left[\sum_{n=1,m=1}^{n=2,m=6}\left(\left(e_{m,n,1,k}\right)^2 + \left(e_{m,n,2,k}\right)^2\right) + \sum_{i=1,j=1}^{m=6}\left(l_{i,j,k}\right)^2\right] \tag{29}$$

Then the iteration error $\boldsymbol{\Delta W}$ of $\boldsymbol{W}$ at time k and time $k+1$ can be calculated.

$$\boldsymbol{\Delta W_k} = -\left(\boldsymbol{J_k^T}(\boldsymbol{W})\,\boldsymbol{J_k}(\boldsymbol{W}) + \boldsymbol{\mu I}\right)^{-1} \boldsymbol{J_k^T}(\boldsymbol{W})\,\boldsymbol{e_k}(\boldsymbol{W}) \tag{30}$$

$$\boldsymbol{W_{k+1}} = \boldsymbol{W_k} + \boldsymbol{\Delta W_k} \tag{31}$$

where $\boldsymbol{J_k}(\boldsymbol{W})$ is the Jacobian matrix of $\boldsymbol{e_k}(\boldsymbol{W})$, I is the unit matrix, and μ is a damping coefficient, which directly decides the convergence rate of the algorithm.

$$\boldsymbol{J_k}(\boldsymbol{W}) = \begin{bmatrix} \frac{\partial e_{1,1,1,k}}{\partial \varphi_{11}} & \cdots & \frac{\partial e_{1,1,1,k}}{\partial X^r_{6gz}} \\ \vdots & \ddots & \vdots \\ \frac{\partial l_{5,6,k}}{\partial \varphi_{11}} & \cdots & \frac{\partial l_{5,6,k}}{\partial X^r_{6gz}} \end{bmatrix}_{39\times 38} \tag{32}$$

The detailed algorithm process is shown in Fig. 5. One thing should be noted is that the adjustment factor γ is constant and $\gamma > 0$. The adjustment factor determines whether L-M algorithm is closer to steepest descent method or Gauss-Newton method, which improves the convergence speed of the algorithm.

2) Calibration Algorithm Based on PSO: PSO is an optimal algorithm based on artificial intelligence and evolutionary computing theory. By following the optimal particles in the solution space, it can obtain the global optimal solution. This algorithm has the advantages of simple concept and easy implementation, also there is no crossover, mutation or other

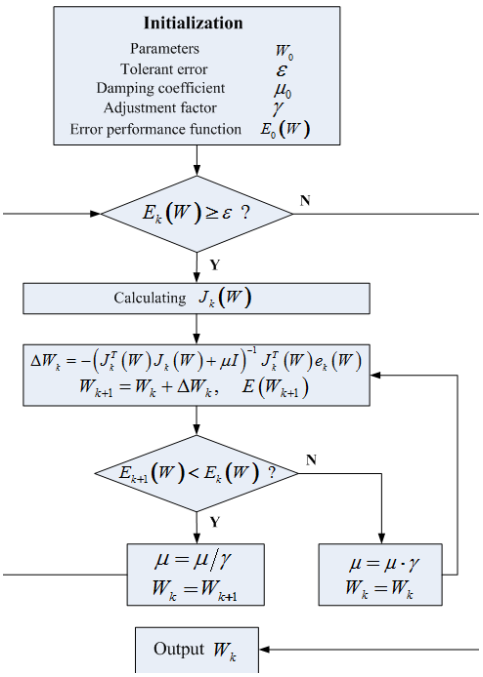

Fig. 5. Process of calibration algorithm based on L-M.

complex operations like genetic algorithm. The calibration algorithm based on PSO is outlined below.

According to the calibration scheme, we can choose Equations (27) as the particle model and Equations (28) as the population evaluation model. Choosing the absolute maximum value in $e(W)$ as the evaluation result, namely:

$$e_{result} = max\,|[\boldsymbol{e}(\boldsymbol{W})]| \tag{33}$$

Assuming that the amount of particles in one population is $popsize$, and taking particle u ($u \in [1, popsize]$) as an example, its position in generation k is $W_{u,k}$, and its speed is $\boldsymbol{S_{u,k}} = \left[s_{u,k,1}, \cdots, s_{u,k,38}\right]^T$. The best evaluation position that it has ever experienced in the past k generations is $\boldsymbol{P_{u,k}} = \left[p_{u,k,1}, \cdots, p_{u,k,38}\right]^T$, and $\boldsymbol{P_{u,k}}$ is determined by the following formula. Also there is a best evaluation position $\boldsymbol{P_{best,k}}$ for all of the $popsize$ particles in the past k generations.

$$\boldsymbol{P_{u,k}} = \begin{cases} \boldsymbol{P_{u,k-1}}, & if\ e_{result,k} \geq e_{result,k-1} \\ \boldsymbol{W_{u,k}}, & otherwise \end{cases} \tag{34}$$

$$\boldsymbol{P_{best,k}} = min\left(\boldsymbol{P_{u,k}}\right), u = 1, \cdots, popsize \tag{35}$$

According to Ref. [22], if the speed and position of particle u are known in generation k, then its speed and position in generation $k+1$ can be expressed as follows.

$$\begin{cases} \boldsymbol{S_{u,k+1}} = \boldsymbol{S_{u,k}} + l_1 h_{u,1}\left(\boldsymbol{P_{u,k}} - \boldsymbol{W_{u,k}}\right) \\ \qquad\qquad + l_2 h_{u,2}\left(\boldsymbol{P_{best,k}} - \boldsymbol{W_{u,k}}\right) \\ \boldsymbol{W_{u,k+1}} = \boldsymbol{W_{u,k}} + \boldsymbol{S_{u,k+1}} \end{cases}, \quad u = 1, \cdots, popsize \tag{36}$$

where l_1 is the weight coefficient of particle u, and l_2 is the global weight coefficient. Usually l_1, l_2 are presupposed constant and $l_1, l_2 \in (0, 2)$. $h_{u,1}, h_{u,2}$ are independent and uniformly distributed random numbers in $[0, 1]$, namely $h_{u,1}, h_{u,2} \in U(0, 1)$.

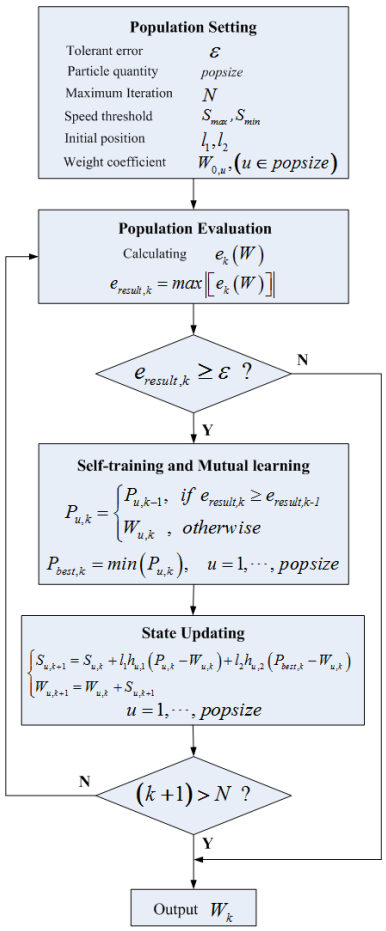

Fig. 6. Process of calibration algorithm based on PSO.

The detailed algorithm process is shown in Fig.6. During state updating, the speed $S_{u,k}$ may be very quick, so it is necessary to judge the speed to ensure a comprehensive search of solution space.

3) Analysis of the Two Calibration Algorithms: Both of the above two algorithms can achieve the calibration of SHPMPS. However, in practical application, they have their own advantages and disadvantages:

(1) **Initialization**. L-M needs to set a relatively accurate initial value to ensure the algorithm convergence, which increases the workload in the preparation stage; PSO only needs to know the range of the initial value, and generates a large number of particles through its algorithm for global search, which reduces the workload in the early stage;

(2) **Computational cost**. The core of calibration algorithm is to solve large nonlinear equations. Aiming at this problem, L-M needs to calculate the Jacobian matrix frequently. However, it brings a large amount of computational cost thanks to the high matrix order. The computational cost of PSO depends on the size of population, so setting a reasonable population can make the computational cost within an acceptable range.

(3) **Calculating true value**. Since the initial value of L-M is around the truth value, the true value can be determined as long as the algorithm converges; As for PSO, the particles are distributed in the whole unsolved space, if the space scale is very large, it may appear the pseudo-truth value after calculating, causing a failed calibration. Therefore, we should try to shrink the range of unsolved space to a reasonable area before using calibration algorithm based on PSO.

According to the analysis above, L-M can achieve the calibration, but it has the problems of large computation and workload. PSO can realize the calibration with a smaller computation by reasonably setting the population and unsolved space, but the pseudo-truth value problem needs to be noted after calibrating. As for which method is better, the subsequent experiments will discuss in detail.

IV. Positioning Algorithm

According to the system working principle, the main purpose of positioning algorithm is to solve Equations (21), and Equations (15) has shown the result by LSE. However, the disturbances such as vibration, light pollution, motor speed fluctuation will generate a large number of gross errors and these gross error will be introduced to the system measuring, which reduces the positioning accuracy. The LSE achieves the optimal unbiased estimation by minimizing the sum of squared residuals, which has a weak ability to eliminate the influence of gross error [23]. Therefore, in order to eliminate the influence of gross error, improve the robustness and measurement accuracy of this system, a new positioning algorithm needs to be further studied.

Maximum likelihood estimation (MLE) is a high-efficiency robust estimation algorithm [24]. By setting the weighting coefficient, this algorithm can reduce the influence of gross error dramatically. In this part, we apply the MLE to the positioning algorithm, and propose a new algorithm to improve the robustness of this system.

Supposing this system is made up of two transmitters, due to the existence of measurement error, the results of the constraint equations in Equations (21) are not always zero. Therefore, Equations (21) can be rewritten as follows:

$$\mathbf{e_i} = b_i - a_i \boldsymbol{X}_{\boldsymbol{g}}^{\boldsymbol{r}} \tag{37}$$

where $\mathbf{e_i}$ is the constraint error, a_i and b_i are the coefficients based on Equations (21).

According to the thought of MLE, in order to obtain the optimal estimation of the receiver coordinates X_g^r, we only need to minimize the constraint error $\mathbf{e_i}$. So the likelihood function is constructed as shown in Equations (38).

$$\mathbf{J}\left(\boldsymbol{X}_{\boldsymbol{g}}^{\boldsymbol{r}}\right) = -\sum_{i=1}^{m=4} \rho_i\left(\mathbf{e}\right) \tag{38}$$

In order to obtain the minimum constraint error $\mathbf{e_i}$, the derivative of Equations (38) is calculated.

$$\begin{aligned} \frac{\partial \mathbf{J}\left(\boldsymbol{X}_{\boldsymbol{g}}^{\boldsymbol{r}}\right)}{\partial \boldsymbol{X}_{\boldsymbol{g}}^{\boldsymbol{r}}} &= -\sum_{i=1}^{m=4} \frac{\partial \rho_i\left(\mathbf{e}\right)}{\partial \mathbf{e_i}} \cdot \frac{\partial \mathbf{e_i}}{\partial\left(\boldsymbol{X}_{\boldsymbol{g}}^{\boldsymbol{r}}\right)} \\ &= \sum_{i=1}^{m=4} a_i \cdot \frac{\partial \rho_i\left(\mathbf{e}\right)}{\partial \mathbf{e_i}} \\ &= \sum_{i=1}^{m=4} a_i \cdot \frac{\mathbf{e_i}}{\mathbf{e_i}} \frac{\partial \rho_i\left(\mathbf{e}\right)}{\partial \mathbf{e_i}} \\ &= \sum_{i=1}^{m=4} a_i \cdot \left(b_i - a_i \boldsymbol{X}_{\boldsymbol{g}}^{\boldsymbol{r}}\right) \frac{1}{\mathbf{e_i}} \frac{\partial \rho_i\left(\mathbf{e}\right)}{\partial \mathbf{e_i}} \end{aligned} \tag{39}$$

Supposing $\psi_i(\mathbf{e}) = \frac{\partial \rho_i(\mathbf{e})}{\partial \mathbf{e_i}}$ is the score function and $q_i(\mathbf{e}) = \frac{\psi_i(\mathbf{e})}{\mathbf{e_i}}$ is the weight function. Setting the derivative Equations (39) equals to zero, and writing the equation in matrix form, we have:

$$\mathbf{A}^T \boldsymbol{Q}\left(\boldsymbol{B} - \boldsymbol{A}\boldsymbol{X}_{\boldsymbol{g}}^{\boldsymbol{r}}\right) = \mathbf{0} \tag{40}$$

where $\boldsymbol{Q} = diag\{q_i(\mathbf{e})\}$, $\boldsymbol{A}$, $\boldsymbol{B}$ is the coefficients matrix based on a_i and b_i.

So the receiver coordinates based on MLE can be obtained as shown below.

$$\boldsymbol{X}_{\boldsymbol{g}}^{\boldsymbol{r}} = \left(\mathbf{A}^T \boldsymbol{Q}\boldsymbol{A}\right)^{-1}\mathbf{A}^T \boldsymbol{Q}\boldsymbol{B} \tag{41}$$

According to Equations (40), we can see the choice of the likelihood function $\rho_i(\mathbf{e})$ directly determines the final estimation results $\boldsymbol{X}_{\boldsymbol{g}}^{\boldsymbol{r}}$. In general, there are three ways to get the likelihood function $\rho_i(\mathbf{e})$, namely IGG method, Huber method and Hample method. In this paper, we use the IGG method as the likelihood function $\rho_i(\mathbf{e})$, as a result, $\rho_i(\mathbf{e})$ is shown as below.

$$\rho_i(\mathbf{e}) = \begin{cases} \mathbf{e_i}^2/2, & |\mathbf{e_i}| < c \\ c|\mathbf{e_i}|, & c < |\mathbf{e_i}| < b \\ d, & b \le |\mathbf{e_i}| \end{cases} \tag{42}$$

where, b, c and d are all constants, and the values of each constant are generally calculated according to experience (For specific methods, please refer to Ref. [25]).

According to Equations (42), the weight function $q_i(\mathbf{e})$ can be calculated. For the measurement without gross error, the weight function $q_i(\mathbf{e}) = 1$, which indicates that this measurement is credible and can be retained, also Equations (41) turns into Equations (15), which means that LSE is a special form of MLE. When the gross error exists, if there is a small gross error, the weight function turns into $q_i(\mathbf{e}) = c/|\mathbf{e}|$, by which the influence of the gross error can be reduce; if there is a large gross error, the weight function becomes $q_i(\mathbf{e}) = 0$, namely, we take this measurement as invalid measurement. In a word, based on this algorithm, we can realize the purpose of resisting gross error, keeping system robustness and improving the positioning accuracy.

V. Results

To verify the effect of proposed calibration method and positioning algorithm, a series of simulations and experiments have been designed and carried out. By simulating the SHPMPS based on two transmitters, the simulation experiments verify the feasibility of the system scheme and the validity of the proposed algorithm in theory; by inventing the SHPMPS prototype, the positioning accuracy of SHPMPS can be tested in a simulated narrow cabin environment.

A. Simulation Experiment

According to the mathematical model in Chap.1.2, we can see the system's errors are directly reflected in the errors of the scanning angles θ_1, θ_2. In order to facilitate the simulation, we establish the system model only with the scanning angle error $\Delta\theta_1, \Delta\theta_2$. Namely, the true relative relationship between the transmitter coordinate system and the global coordinate system are directly given, that is, we suppose the two transmitters' true external parameters and internal parameters are known. Meantime the receivers' true coordinates in the global coordinate system are also known, so the pitch angle and azimuth angle of a receiver relative to a transmitter can be calculated, and then the scanning angles θ_1, θ_2 of the transmitter sweeping the receiver can be calculated by Equations (8). The scanning angle errors $\Delta\theta_1$, $\Delta\theta_2$ are added into the obtained scanning angles θ_1, θ_2 to simulate the actual working state of this system. Based on the scanning angles with errors, the calibration method and positioning algorithm can be tested.

TABLE I
THE EXPERIMENTAL CONDITIONS OF TWO CALIBRATION SCHEME

Basic Parameters	
T1	Coordinate(m) (0,0,0) Attitude angle(°) (0,0,0) Internal parameters:$\varphi_1 = 45°$, $\varphi_2 = -45°$, $\theta_{off} = -90°$, $\Delta z = 0.1$mm
T2	Coordinate(m) (10,0,0) Attitude angle(°) (0,0,0) Internal parameters:$\varphi_1 = 45°$, $\varphi_2 = -45°$, $\theta_{off} = -90°$, $\Delta z = 0.1$mm
Scanning angle error(″)	$15+0\times randn$ [a]
The distance constraint scheme [b]	
	$d_{1,2} = 400.00$ $d_{1,3} = 300.00$ $d_{1,4} = 500.00$ $d_{1,5} = 600.00$ $d_{1,6} = 721.11$ $d_{2,3} = 500.00$ $d_{2,4} = 300.00$ $d_{2,5} = 721.11$ $d_{2,6} = 600.00$ $d_{3,4} = 400.00$ $d_{3,5} = 300.00$ $d_{3,6} = 500.00$ $d_{4,5} = 500.00$ $d_{4,6} = 300.00$ $d_{5,6} = 400.00$
The receiver coordinates constraint scheme[c]	
	R_1 (5000.00, 10000.00, 100.00) R_2 (4600.00, 10000.00, 100.00) R_3 (5000.00, 10000.00, 400.00) R_4 (4600.00, 10000.00, 400.00) R_5 (5000.00, 10000.00, 700.00)

[a] The scanning angle error consists of constant error and random error to simulate the real working state, and "$rand$" stands for a random number with a mean of zero and a variance of one;
[b] "$d_{i,j}$" stands for the distance between Receiver i and Receiver j, and the unit is millimeter;
[c] "R_i" stands for the coordinates of Receiver i, and the unit is millimeter.

TABLE II
THE CALIBRATION RESULTS OF TWO CALIBRATION SCHEME[D]

Transmitter Number	Calibration Parameters	Theoretical Value	Distance Constraint	Coordinates Constraint
T1	Coordinate(m)	(0,0,0)	(0,0,0)	(0,0,0)
	Attitude angle(°)	(0,0,0)	(0.00388,-0.00645,-0.01333)	(0.00065, 0.00009, 0.00186)
	inclined angle1(φ_1) (°)	45.00000	45.00454	45.00663
	inclined angle2(φ_2) (°)	-45.00000	-44.99134	-44.99538
	offset angle(θ_{off})(°)	-90.00000	-89.99921	-90.00072
	biased error(Δz)(mm)	0.100	0.095	0.097
T2	Coordinate(m)	(10,0,0)	(10.00024,0.00000,-0.00028)	(9.99999,0.00000,-0.00004)
	Attitude angle(°)	(0,0,0)	(0.00382,0.00036,0.00197)	(0.01182,0.00342,-0.02034)
	inclined angle1(φ_1) (°)	45.00000	44.99853	44.99421
	inclined angle2(φ_2) (°)	-45.00000	-44.99762	-45.00655
	offset angle(θ_{off})(°)	-90.00000	-89.99952	-90.00087
	biased error(Δz)(mm)	0.100	0.095	0.100

[d] The tolerant error ε is 10^{-8} in the calibration algorithm based on L-M.

1) Calibration Scheme Experiment: There are two calibration scheme mentioned in Chap.2, which are based on the known distance or the known receiver coordinates, respectively. Considering the narrow cabin, the distance constraint scheme was finally selected in Chap.2. However, for other application scenarios, the receiver coordinates constraint scheme may be available, so the validity of both schemes needs to be analyzed. The experimental conditions of the two calibration scheme are shown in Table I, and the calibration algorithm based on L-M is used to realize the calibration and the calibration results are shown in Table II.

Theoretically, the calibration results should be equal to the theoretical value, while the system random error causes the differences between the calibration results and the theoretical value. However, we cannot judge the merits of the two methods only from the calibration error in Table II, because there are no significant differences in the calibration results for these two calibration schemes, they are just different from the theoretical values. In addition, it should be noted that the coordinates of T_1 obtained by the two calibration scheme are all equal to the theoretical values. This is because the origin of transmitter 1 coordinate system is taken as the origin of the global coordinate system when the global coordinate system is established.

TABLE III
THE POSITIONING RESULTS BASED ON TWO SCHEMES (UNIT: MILLIMETER)

Receiver Number	TRUE Position	Theoretical Value	Error1	Distance Constraint	Error2	Coordinates Constraint	Error3
R1	(5000.00, 10000.00, 100.00)	(4998.89, 10000.16, 100.05)	(1.11, 0.16, 0.05)	(4998.83, 10000.13, 99.99)	(1.17, 0.13, 0.01)	(4999.03, 9999.70, 100.12)	(0.97, 0.30, 0.12)
R2	(4600.00, 10000.00, 100.00)	(4598.91, 9999.84, 100.05)	(1.09, 0.16, 0.05)	(4598.82, 9999.99, 99.99)	(0.95, 0.01, 0.01)	(4598.92, 9999.82, 100.12)	(1.08, 0.18, 0.12)
R3	(5000.00, 10000.00, 400.00)	(4998.89, 9999.81, 400.04)	(1.11, 0.19, 0.04)	(4998.84, 9999.98, 400.01)	(1.16, 0.02, 0.01)	(4998.96, 9999.65, 400.11)	(1.04, 0.35, 0.11)
R4	(4600.00, 10000.00, 1000.00)	(4598.92, 9999.95, 1000.05)	(1.08, 0.05, 0.05)	(4598.97, 9999.54, 1000.02)	(1.03, 0.46, 0.02)	(4599.05, 9999.23, 1000.04)	(0.95, 0.77, 0.04)
R5	(5000.00, 10000.00, 1000.00)	(4998.87, 10000.11, 1000.06)	(1.13, 0.11, 0.06)	(4999.01, 9999,74, 1000.03)	(0.99, 0.26, 0.03)	(4998.97, 9999.42, 1000.06)	(1.03, 0.58, 0.06)
R6	(4600.00, 10000.00, 700.00)	(4598.93, 10000,05, 700,05)	(1.07, 0.05, 0.05)	(4568.89, 9999.86, 700.03)	(1.11, 0.14, 0.03)	(4598.95, 9999.60, 700.09)	(1.05, 0.40, 0.09)
ME		(1.10,0.12,0.05)		(1.11,0.17,0.02)		(1.02,0.43,0.09)	
Total ME		1.10		1.12		1.11	
STD		(0.45,0.05,0.02)		(0.45,0.09,0.01)		(0.42,0.19,0.04)	
Total STD		0.45		0.46		0.46	

To verify the validity of the two schemes, we bind the obtained calibration parameters in Table II into the positioning algorithm based on LSE and use the positioning error to evaluate the two schemes. Table III shows the positioning results using the theoretical calibration parameters, distance constraint calibration parameters and coordinate constraint calibration parameters, respectively. Error 1, Error 2 and Error 3 stand for the absolute value of the difference between the true position and the theoretical value, the true position and the distance constraint value, the true position and the coordinates constraint value, respectively. In different axes of different reveiver, the error $\Delta R(\Delta X, \Delta Y, \Delta Z)$ is obtained by Equations (43). The mean errors (ME) are the mean value of Error 1, Error 2 and Error 3, also the total mean error Δd is obtained by Equations (44). The standard deviation(STD) $R_{std}\,(X_{std}, Y_{std}, Z_{std})$ is obtained by Equations (45) and the total standard deviation d_{std} is obtained by Equations (46).

$$\Delta R = |R_{true} - R_{calculative}| \tag{43}$$

$$\Delta d = \sqrt{\Delta X^2 + \Delta Y^2 + \Delta Z^2} \tag{44}$$

where R_{true} is the true position coordinates of this point, and $R_{calculative}$ is the calculative coordinates.

$$R_{std} = \sqrt{\Delta R_1^2 + \Delta R_2^2 + \cdots + \Delta R_6^2} \Big/ 6 \tag{45}$$

$$d_{std} = \sqrt{X_{std}^2 + Y_{std}^2 + Z_{std}^2} \tag{46}$$

The coordinates of R_1-R_3 have been used for coordinates' constraint calibration, so the positioning results of these three receivers should be better than other receivers in theory, however, from Table III, there are no significant error differences among the six receivers. Moreover, the coordinates of R_4-R_6 are chosen in random, which suggests the coordinates of the whole space can be measured in a small error. Also the total error and the standard deviation of the two scheme are closed to the theoretical result. Based on the analysis above, it can be proved that the two calibration schemes are both valid and accurate.

By analyzing the positioning results of the two schemes, the total mean error of distance constraint is 1.12mm, and the total mean error of coordinates' constraint is 1.11mm, which can prove that the coordinates' constraint scheme is a little more accurate than the distance constraint scheme. That is because there are fewer unknown parameters in the coordinates constraint scheme, and if the receivers' coordinates are known, the distance constraint equations can be written easily, which further decrease the difficulty of solving equations. However, as mentioned in Chap.2, the condition of narrow cabin limits the application of this scheme, so if there is a stable space such as calibration workshop, this scheme will make a huge difference.

TABLE IV
THE CALIBRATION RESULTS BASED ON L-M AND PSO[E]

Transmitter Number	Calibration Parameters	Theoretical Value	L-M	PSO
T1	Coordinate(m)	(0,0,0)	(0,0,0)	(0,0,0)
	Attitude angle(°)	(0,0,0)	(0.00388,-0.00645,-0.01333)	(-0.00341,-0.00054,-0.00049)
	inclined angle1(φ_1) (°)	45.00000	45.00454	45.00162
	inclined angle2(φ_2) (°)	-45.00000	-44.99134	-44.99848
	offset angle(θ_{off})(°)	-90.00000	-89.99921	-89.99932
	biased error(Δz)(mm)	0.100	0.095	0.098
T2	Coordinate(m)	(10,0,0)	(10.00024,0.00000,-0.00028)	(10.00020,0.00000,-0.00001)
	Attitude angle(°)	(0,0,0)	(0.00382,0.00036,0.00197)	(-0.00271,0.00100,-0.00165)
	inclined angle1(φ_1) (°)	45.00000	44.99853	44.99946
	inclined angle2(φ_2) (°)	-45.00000	-44.99762	-45.00216
	offset angle(θ_{off})(°)	-90.00000	-89.99952	-89.99974
	biased error(Δz)(mm)	0.100	0.095	0.100

[E]The tolerant error ε is 10^{-8} in L-M algorithm and PSO algorithm, and the maximum iteration is not used in PSO algorithm.

2) Calibration Algorithm Experiment: Through the experiments above, the validity of the calibration algorithm has been verified. This part mainly tests the calibration accuracy of the two proposed algorithms, and finally the algorithm with better calibration performance will be chosen as the calibration algorithm of SHPMPS.

Similar to the calibration scheme experiment, the calibration algorithm experiment uses the distance constrained calibration scheme and positioning algorithm based on LSE, and the distinction is different calibration algorithm. The experimental conditions are consistent with Table I, and the calibration results and positioning results are shown in Table IV and Table V, respectively. Since the experiment process of the calibration algorithm based on L-M is the same as that in Chap. 4.1.1, the previous results in Table II and Table III are directly used in Table IV and Table V.

According to Table IV, the calibration results based on PSO is closer to the theoritical value than the calibration results based on L-M, which shows the calibration algorithm based on PSO has a better calibration results. As a result, these calibration results cause the total positioning accuracy of PSO is slightly higher than that of L-M by 0.01mm in mean error and standard deviation in Table V, which shows the PSO is better than L-M in accuracy and stability.

The number of iterations to reach the tolerant error has been counted, whose aim is to compare the computational cost of these two algorithms, and the result is shown in Table VI.

According to Table VI, due to the initial parameters information is very close to the real values, there are a few iterations to realize calibration algorithm based on L-M and PSO, and the great initial parameters make the PSO search in a small space which widely decreases the computational cost, also avoids the situation of pseudo-truth value.

Based on the analysis above, the calibration algorithm based on PSO is better than the calibration algorithm based on L-M in computational cost and calibration accuracy, so the calibration algorithm based on PSO is chosen as the practical calibration algorithm of SHPMPS.

TABLE V
THE POSITIONING RESULTS BASED ON L-M AND PSO (UNIT: MILLIMETER)

Receiver Number	TRUE Position	L-M	Error1	PSO	Error2
R1	(5000.00, 10000.00, 100.00)	(4998.83, 10000.13, 99.99)	(1.17, 0.13, 0.01)	(4998.88, 10000.24, 100.00)	(1.12, 0.24, 0.00)
R2	(4600.00, 10000.00, 100.00)	(4598.82, 9999.99, 99.99)	(0.95, 0.01, 0.01)	(4598.92, 10000.00, 100.00)	(1.08, 0.00, 0.00)
R3	(5000.00, 10000.00, 400.00)	(4998.84, 9999.98, 400.01)	(1.16, 0.02, 0.01)	(4998.87, 10000.22, 400.00)	(1.13, 0.22, 0.00)
R4	(4600.00, 10000.00, 1000.00)	(4598.97, 9999.54, 1000.02)	(1.03, 0.46, 0.02)	(4598.99, 9999.78, 999.97)	(1.01, 0.22, 0.03)
R5	(5000.00, 10000.00, 1000.00)	(4999.01, 9999,74, 1000.03)	(0.99, 0.26, 0.03)	(4998.90, 9999.97, 999.99)	(1.10, 0.03, 0.01)
R6	(4600.00, 10000.00, 700.00)	(4568.89, 9999.86, 700.03)	(1.11, 0.14, 0.03)	(4598.85, 9999.94, 699.99)	(1.15, 0.06, 0.01)
ME		(1.11,0.17,0.02)		(1.10,0.13,0.01)	
Total ME		1.12		1.11	
STD		(0.45,0.09,0.01)		(0.45,0.07,0.01)	
Total STD		0.46		0.45	

TABLE VI
THE NUMBER OF ITERATIONS BASED ON L-M AND PSO

	L-M	PSO
Number of iterations	5	3

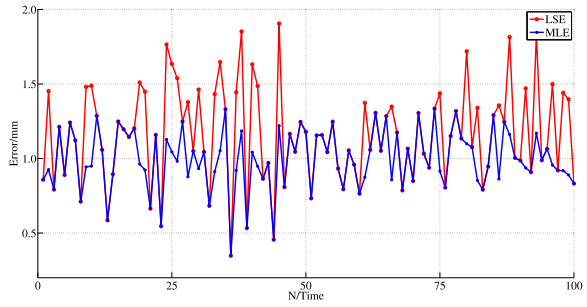

Fig. 7. The positioning error (Δd) comparison of MLE and LSE.

3) Positioning Algorithm Experiment: This section mainly verifies the accuracy and the ability of resisting gross error for these two positioning algorithms. To ensure the fairness of this experiment, the calibration parameters use the results from Table IV with the calibration algorithm of PSO.

At first, the ability of resisting gross error is tested. Let the simulation system measures a fixed point (R6(4600.00,10000.00,700.00))for 100 times using two algorithms, respectively. Random simulation interference is added during this experiment, which is realized by setting $\Delta\theta_1$, $\Delta\theta_2$ in Table I as $15'' + 5'' \times rand$. Fig. 7 and Table VII show the positioning error(Δd), ME and STD of these two algorithms, respectively.

From Fig. 7, when the gross error appears, the positioning algorithm based on LSE does nothing for the gross error, while the positioning algorithm based on MLE reduces the right of the error. This makes the MLE obtains a better result, such as Time 24, Time 38, Time 45 and so on. When there is no gross error, MLE turns into LSE, as a result, the two algorithm get the same positioning result,, such as Time 8, Time 13, Time 23 and so on. According to Table VII, due to the gross error has been processed by MLE, the ME and STD of MLE are better than that of LSE. These prove the positioning algorithm based on MLE is stable and robust, which is consistent with the previous analysis.

TABLE VII
THE ME AND STD OF MLE AND LSE (UNIT: MILLIMETER)

	MLE	LSE
ME	0.99	1.15
STD	0.20	0.32

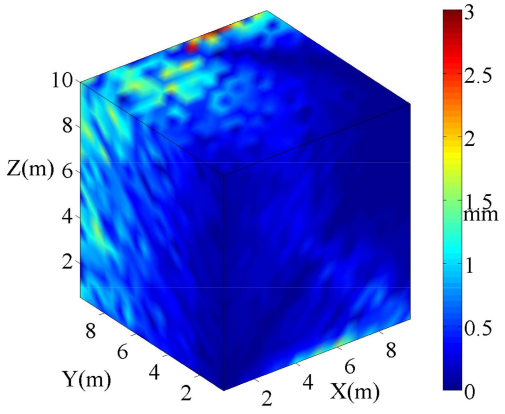

Fig. 8. The positioning error(Δd) with LSE in the whole space.

In the above analysis, we only select one random point to verify the effectiveness of the two positioning algorithm, which is not representative. In order to comprehensively verify the positioning effect of the proposed algorithm, we carry out a full-space positioning experiment, namely, the SHPMPS's positioning accuracy in the whole narrow cabin is measured. The calibration parameters also use the results from Table IV with PSO. The measuring zone is a cuboid with 10m in X-axis, 10m in Y-axis and 10m in Z-axis, and two transmitters are located at (0,0,0) and (10.0002,0,0.00001), respectively. During the whole simulation experiment, the scanning angle errors $\Delta\theta_1$, $\Delta\theta_2$ are still $15'' + 5'' \times rand$. The results are shown in Fig. 8-Fig. 9 and the mean errors of total space and $Y = 10$ are shown in Table VIII.

From Fig. 8 and Fig. 9, we can see that the error is different in different place, which can reflect that the positioning error is related to the layout of the receiver. Also this conclusion can explain why the errors in Table III and Table V are various although the algorithm is same; As the receiver is further away from the transmitters, the positioning error becomes larger and larger. This is caused by the fanned opening angle and the scanning angle error of the laser planes which cannot be avoided. Since the cross profile of the laser plane is cuneal, with the increase of the measuring distance, the intersection area of the laser planes gets bigger, as a result the positioning accuracy becomes poor; The spots in Fig. 8 and Fig. 9 are caused by the random variable of the scanning angle error,

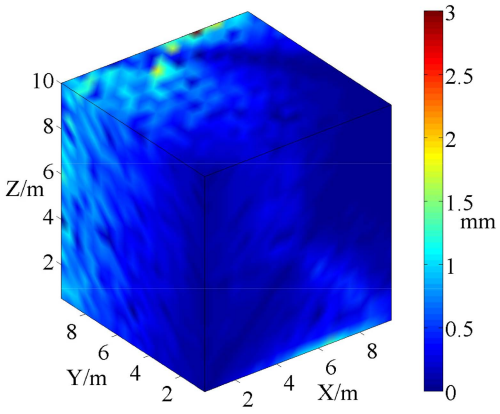

Fig. 9. The positioning error(Δd) with MLE in the whole space.

TABLE VIII
THE MEAN ERROR OF MLE AND LSE

	MLE	LSE
ME (Total Space)	0.46	0.55
ME (Y=10)	0.93	1.11

since MLE has dealed with the gross error of the scanning angle, the positioning error in Fig. 9 looks much smoother than that in Fig. 8. This proves the robustness of MLE again.

According to Table VIII, the mean error of the plane at $Y = 10$ is 1.11, which is consistent with the results in Table V and Table VII; The average total positioning error is 0.46mm with MLE and 0.55mm with LSE, which can reflect the positioning algorithm based on MLE is better than that of LSE in measuring accuracy.

In conclusion, we choose MLE as SHPMPS's positioning algorithm.

B. Verification Experiment

The SHPMPS (as shown in Fig. 10) has been invented to verify the validity of the working principle, calibration method and positioning algorithm. The whole experiment scenario is shown as Fig. 11: A SHPMPS with two transmitters is placed in a simulated narrow cabin nearly 10m×10m×10m, and the calibration equipment is also mounted in the cabin and can be seen by two transmitters. The two transmitters are about 10m apart. Since the positioning accuracy of Leica AT901-LR laser tracker is $\pm 15\mu$m+6μm/m [26], which is higher than the simulation result of SHPMPS, so we take the laser tracker as the reference facility. One thing needs to be explained is that there are nine receivers in the calibration equipment, and we choose the six receivers in the aluminium plate as the calibration points and the remaining three receivers are the points to be measured. All of the receivers' coordinates are measured by the laser tracker as the reference value.

1) Sensor Accuracy Verification Experiment: After completing the initialization of SHPMPS, the receivers' coordinates are located by the laser tracker as the reference results (as shown in Table IX); Then the two transmitters' external and internal parameters can be obtained after calibrating by the calibration equipment; At last the coordinates of the receivers

Fig. 10. SHPMPS.

Fig. 11. Verification experiment environment.

TABLE IX
THE REAL RECEIVERS COORDINATES

Number	Coordinates
R1	(4849.02,10260.48,449.52)
R2	(5209.03,10130.52,459.48)
R3	(4869.00,10250.49,269.51)
R4	(5199.02,10140.52,294.48)
R5	(4818.99,10250.48,119.52)
R6	(5248.99,10140.52,114.48)
R7	(4828.96,10230.48,-130.48)
R8	(5278.98,10130.53,-105.53)
R9	(5039.03,10200.50,509.49)

can be confirmed using the SHPMPS. We choose R1-R6 to form the calibration equipment, and R4-R9 as the points to be measured. Through comparing the measured coordinates and the reference coordinates of the 6 receivers, the positioning accuracy of SHPMPS can be evaluated. To verify the calibration algorithm and positioning algorithm mentioned above, the measurement experiments have been repeated four times, which use L-M and LSE, L-M and MLE, PSO and LSE, PSO and MLE, respectively. The rotation frequency of the two transmitters is set at 50Hz, so the output frequency of SHPMPS can reach 50Hz, and we choose the one seconds smooth measuring result as the receiver's measuring coordinates. The positioning errors are shown as Table X.

According to Table X, the validity of the working principle, calibration method and positioning algorithm can be verified.

TABLE X
THE POSITIONING ACCURACY FOR FOUR EXPERIMENTS (UNIT: MILLIMETER)

Receiver Number	Error	R4	R5	R6	R7	R8	R9	*Average*	*Std*
L-M & LSE	ΔX	1.20	1.20	1.15	1.18	1.18	1.19	1.18	0.48
	ΔY	0.04	0.04	0.05	0.03	0.05	0.01	0.04	0.02
	ΔZ	0.05	0.05	0.05	0.05	0.05	0.05	0.05	0.02
	Δd	1.21	1.20	1.15	1.18	1.19	1.19	1.19	0.48
L-M & MLE	ΔX	1.03	1.06	0.99	1.02	1.03	1.00	1.02	0.42
	ΔY	0.03	0.03	0.04	0.03	0.03	0.01	0.03	0.01
	ΔZ	0.05	0.05	0.05	0.05	0.05	0.05	0.05	0.02
	Δd	1.03	1.06	0.99	1.02	1.03	1.00	1.02	0.42
PSO & LSE	ΔX	1.18	1.13	1.13	1.13	1.20	1.17	1.16	0.47
	ΔY	0.04	0.03	0.05	0.03	0.06	0.01	0.04	0.02
	ΔZ	0.05	0.05	0.05	0.05	0.05	0.05	0.05	0.02
	Δd	1.18	1.13	1.13	1.13	1.20	1.18	1.16	0.47
PSO & MLE	ΔX	1.00	1.00	0.96	1.00	0.98	1.03	1.00	0.41
	ΔY	0.03	0.03	0.04	0.03	0.05	0.01	0.03	0.01
	ΔZ	0.05	0.05	0.05	0.05	0.05	0.05	0.05	0.02
	Δd	1.00	1.00	0.97	1.01	0.99	1.03	1.00	0.41

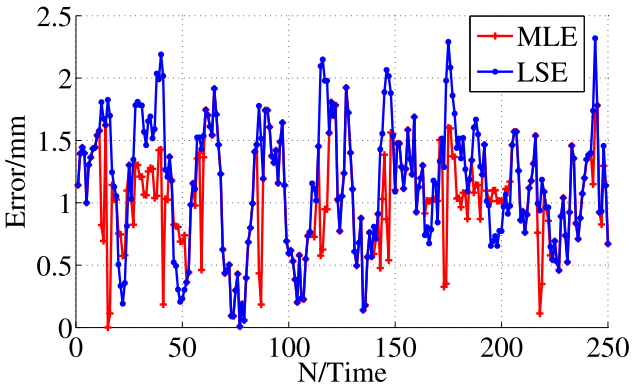

Fig. 12. The positioning results under external interference.

Through comparing the positioning errors of the four experiments, the positioning accuracy of the PSO calibration algorithm is better than that of the L-M calibration algorithm at about 0.03mm in total and the positioning accuracy of the MLE positioning algorithm is better than that of the LSE positioning algorithm at about 0.16mm in total, also the standard deviation shows the same result at the aspect of stability. These are consistent with the analysis and simulation results above. As a result, the system's positioning accuracy of SHPMPS can reach 1.00mm in total with PSO calibration algorithm and MLE positioning algorithm.

Since the receivers can just be placed at limited positions, so the positioning accuracy at every point in the whole place cannot be confirmed. As a result, the whole space's positioning accuracy cannot be verified which is a great pity. However, according to the positioning results above, we have reasons to believe that the positioning accuracy of this system can reach sub-millimeter level in the narrow cabin.

2) Anti-Interference Experiment: To further verify SHPMPS's stability of resisting gross error, one more experiment which is like the above four experiments is carried out. There are two differences between this experiment and the former experiments: One is that during the whole experiment, we added the random vibration interference to the two transmitters by shaking the transmitters slightly, and another is that we only choose one receiver at random (R9) for repeated measuring. The calibration algorithm used PSO, and the positioning algorithm used LSE and MLE, respectively.

TABLE XI
THE ME AND STD OF MLE AND LSE (UNIT: MILLIMETER)

	MLE	LSE
ME	1.02	1.18
STD	0.42	0.53

The rotation frequency of the two transmitters is still set at 50Hz, and the experiment lasts for 5s. The results are shown as Fig. 12.

According to Fig. 12, compared with LSE, the measuring results of MLE are more stable and accurate. Table XI counts the ME and the STD of these two algorithms' positioning error (Δd), according to this table, the statistical results prove the robustness and accuracy of MLE again.

To sum it up, the SHPMPS has been verified in working principle, calibration method, positioning algorithm and anti-interference adaptability.

VI. CONCLUSION

This paper presents an integrated system called SHPMPS for key points measuring in confined cabins. In this system, the key points' coordinates are measured by the transmitters and receivers based on the theodolite principle. The calibration equipment is used as an orienting device, and the relative relation of transmitter coordinate system and global coordinate system is established by the calibration algorithm. Through the positioning algorithm in the front-end processor, the coordinates can be gotten and shown in the computer. For this system, although the mathematical principle is not a new one, the high frequency output scheme based on high-speed motor is quite fresh. Additionally, the construction of the calibration equipment plays a pivotal role and a convenient and fast calibration scheme is carried out. As a result, the relationship of the coordinates system and the parameters of SHPMPS can be determined at one time. Besides, through the robust positioning algorithm based on MLE, the coordinates can be measured whether there are external disturbances or not. To verify the validity of the invented system, a series of simulation and verification experiments have been designed and conducted, and the results show that the PSO calibration algorithm and the MLE positioning algorithm have the best effect for this system and based on these algorithms the positioning accuracy can reach 1.00mm in total, which can meet the needs of positioning in the narrow cabin. To evaluate the system's ability in anti-interference, a verification experiment with vibration interference has been developed and the accuracy has been presented. The results show that the positioning accuracy can still keep in nearly 1.00mm with a high output frequency at 50Hz, which has verified the great environmental suitability for SHPMPS.

The positioning results have demonstrated that the integrated system exhibits a good accuracy which can fully meet the needs of positioning in narrow cabin. It is believed that the proposed scheme is quite high-efficient and easy to be implemented. It is suitable for the high-frequency and narrow-space measurement. Future work will focus on the improvement of measuring accuracy with more transmitters and the layout rules of transmitters.

ACKNOWLEDGMENT

The authors would like to thank the help given by Xiang Jin and Na Liu in system development. In addition, Qiang Hao would like to thank Yanli Gao for her encouragement and support over the past years.

REFERENCES

[1] L. K. Wook and N. Byeong, "A study on smart accuracy control system based on augmented reality and portable measurement device for shipbuilding," *J. Comput. Struct. Eng. Inst. Korea*, vol. 32, pp. 65–74, 2019.
[2] B.-R. Park and H.-C. Kim, "Development of cell guide quality management system for container ships," *J. Ocean Eng. Technol.*, vol. 32, no. 3, pp. 158–165, Jun. 2018.
[3] K.-Y. Kwon, "A study on the applications of measurement systems for dimensional quality management in shipbuilding," *Korean J. Comput. Des. Eng.*, vol. 22, no. 3, pp. 317–328, Sep. 2017.
[4] O. Blanco-Novoa, T. M. Fernandez-Carames, P. Fraga-Lamas, and M. A. Vilar-Montesinos, "A practical evaluation of commercial industrial augmented reality systems in an industry 4.0 shipyard," *IEEE Access*, vol. 6, pp. 8201–8218, 2018.
[5] A. Mendikute, J. A. Yagüe-Fabra, M. Zatarain, Á. Bertelsen, and I. Leizea, "Self-calibrated in-process photogrammetry for large raw part measurement and alignment before machining," *Sensors*, vol. 17, no. 9, p. 2066, Sep. 2017.
[6] B. Sun, J. Zhu, L. Yang, S. Yang, and Y. Guo, "Sensor for in-motion continuous 3D shape measurement based on dual line-scan cameras," *Sensors*, vol. 16, no. 11, p. 1949, Nov. 2016.
[7] B. Sun, J. Zhu, L. Yang, S. Yang, and Z. Niu, "Calibration of line-scan cameras for precision measurement," *Appl. Opt.*, vol. 55, no. 25, pp. 6836–6843, 2016.
[8] H. Du, X. Chen, J. Xi, C. Yu, and B. Zhao, "Development and verification of a novel robot-integrated fringe projection 3D scanning system for large-scale metrology," *Sensors*, vol. 17, no. 12, p. 2886, Dec. 2017.
[9] Z. D. D. Hui and X. Chen, "Integrated fringe projection 3D scanning system for large-scale metrology based on laser tracker," *Proc. SPIE*, vol. 10458, Oct. 2017, Art. no. 104581T.
[10] Z. H. Z. Zhang and J. Zhu, "Laser automatic theodolite measurement system based on vision guidance," *J. Optoelectron. Laser*, vol. 22, pp. 115–119, 2011.
[11] Z. Zhang, J. Zhu, H. Zhou, and S. Ye, "The guidance methodology of a new automatic guided laser theodolite system," *Proc. SPIE*, vol. 7160, Feb. 2009, Art. no. 71600R.
[12] Y. Yang, C. Zhang, J. Lu, and H. Zhang, "The optical reference error analysis and control method in ground validation system of stellar-inertial integration," *IEEE Sensors J.*, vol. 19, no. 2, pp. 670–678, Jan. 2019.
[13] H. Deng, K. Yang, Q. Quan, and K.-Y. Cai, "Accurate and flexible calibration method for a class of visual sensor networks," *IEEE Sensors J.*, vol. 20, no. 6, pp. 3257–3269, Mar. 2020.
[14] Q. Fu *et al.*, "A robust RGB-D SLAM system with points and lines for low texture indoor environments," *IEEE Sensors J.*, vol. 19, no. 21, pp. 9908–9920, Nov. 2019.
[15] Y. Shen and Y. Dai, "Fast automatic differentiation for large scale bundle adjustment," *IEEE Access*, vol. 6, pp. 11146–11153, 2018.
[16] Z. Liu, X. Zhang, M. Su, Y. Sun, H. Han, and P. Wang, "Convergence analysis of Newton-raphson method in feasible power-flow for DC network," *IEEE Trans. Power Syst.*, vol. 35, no. 5, pp. 4100–4103, Sep. 2020.
[17] M. Cosovic and D. Vukobratovic, "Distributed Gauss–Newton method for state estimation using belief propagation," *IEEE Trans. Power Syst.*, vol. 34, no. 1, pp. 648–658, Jan. 2019.
[18] Q. Li, J. Wu, Y. Chen, J. Wang, S. Gao, and Z. Wu, "A new response approximation model of the quadrant detector using the optimized BP neural network," *IEEE Sensors J.*, vol. 20, no. 8, pp. 4345–4352, Apr. 2020.
[19] D. G. Silva and R. Attux, "Simulated annealing for independent component analysis over galois fields," *IEEE Signal Process. Lett.*, vol. 25, no. 4, pp. 516–520, Apr. 2018.
[20] S. H. Hojjati, A. Ebrahimzadeh, M. Najimi, and A. Reihanian, "Sensor selection for cooperative spectrum sensing in multiantenna sensor networks based on convex optimization and genetic algorithm," *IEEE Sensors J.*, vol. 16, no. 10, pp. 3486–3487, May 2016.
[21] Y. Morsly, N. Aouf, M. S. Djouadi, and M. Richardson, "Particle swarm optimization inspired probability algorithm for optimal camera network placement," *IEEE Sensors J.*, vol. 12, no. 5, pp. 1402–1412, May 2012.
[22] Z. J. K. Xu and Z. Chen, "Layout design method of star sensor based on particle swarm optimization algorithm," *J. Jilin Univ.*, vol. 49, pp. 972–978, 2019.
[23] L.-Q. Li, W.-X. Xie, and Z.-X. Liu, "Auxiliary truncated particle filtering with least-square method for bearings-only maneuvering target tracking," *IEEE Trans. Aerosp. Electron. Syst.*, vol. 52, no. 5, pp. 2562–2567, Oct. 2016.
[24] I. Tolic, K. Milicevic, N. Suvak, and I. Biondic, "Non-linear least squares and maximum likelihood estimation of probability density function of cross-border transmission losses," *IEEE Trans. Power Syst.*, vol. 33, no. 2, pp. 2230–2238, Mar. 2018.
[25] W. Zhou, "The classical error theory and estimation," *Acta Geodaetica et Cartographica Sinica*, vol. 18, no. 2, pp. 115–120, 1989.
[26] S. Yin, Y. Ren, Y. Guo, J. Zhu, S. Yang, and S. Ye, "Development and calibration of an integrated 3D scanning system for high-accuracy large-scale metrology," *Measurement*, vol. 54, pp. 65–76, Aug. 2014.

Qiang Hao was born in 1992. He received the B.S. degree from the Department of Automation, Harbin Engineering University, Harbin, China, in 2015. He is currently pursuing the Ph.D. degree in instruments science and technology with the Harbin Institute of Technology. His current research interests include inertial navigation systems and indoor positioning systems.

Guochen Wang received the B.Eng. and Ph.D. degrees from Harbin Engineering University, Harbin, China, in 2010 and 2016, respectively. He is currently a Postdoctoral Researcher with the School of Instruments Science and Technology, Harbin Institute of Technology, Harbin. His current research interests include inertial navigation systems and fiber-optics gyroscope.

Pan Jiang received the bachelor's degree from Harbin Engineering University, China, in 2015. He is currently pursuing the Ph.D. degree with the Harbin Institute of Technology. His main research direction is high-precision inertial navigation algorithm.

Dongkang Yu received the master's degree from Beihang University, China, in 2018. He is currently an Engineer with the China Ship Research and Development Academy. His main research direction is high-precision inertial navigation algorithm.

Dan Wang received the master's degree from Harbin Engineering University, China, in 2010. She is currently a Senior Engineer with the China Ship Research and Development Academy. Her main research direction is high-precision inertial navigation algorithm.

Ming Yang received the master's degree from the Stevens Institute of Technology, Hoboken, NJ, USA, in 2013. He is currently an Engineer with the China Ship Research and Development Academy. His main research direction is high-precision inertial navigation algorithm.

Dingjie Xu was born in April 1966. He is a Professor and a Ph.D. Tutor with the Institute of Navigation Instrument, Harbin Institute of Technology. He is also mainly invloved in teaching and research in navigation, guidance, and control.